Dynamics of a Bis-intercalator DNA Complex by ^{1}H-Detected Natural Abundance ^{13}C NMR Spectroscopy†

H. Peter Spielmann*

Departments of Biochemistry and Chemistry, and the Kentucky Center for Structural Biology, University of Kentucky, Lexington, Kentucky 40536-0084

Received April 8, 1998; Revised Manuscript Received October 5, 1998

ABSTRACT: The dynamics of the DNA oligomer d(CGCTAGCG)$_2$ (CTSYM) and its complex with the dye 1,1-(4,4,8,8-tetramethyl-4,8-diazaundecamethylene)-bis-4-(3-methyl-2,3-dihydro-(benzo-1,3-thiazole)-2-methylidene)-quinolinium tetraiodide (TOTO) (CTSYMTOTO) bis-intercalated at the 5′-CT-3′ sequence steps have been determined from NMR relaxation parameters. Longitudinal and transverse ^{13}C relaxation rates and heteronuclear NOE relaxation data were acquired and have been analyzed in the context of the Lipari and Szabo model-free formalism. The overall rotational correlation time for the CTSYM is 3.44 ns and the CTSYMTOTO is 3.48 ns. The generalized order parameters (S^2) for methine carbons in the CTSYM and CTSYMTOTO are relatively high but nonuniform for the molecules and show sequence context and conformation-dependent variations. Average values of $S^2 = 0.79 \pm 0.02$ for the CTSYM, $S^2 = 0.80 \pm 0.04$ for the CTSYMTOTO aromatic spins, $S^2 = 0.76 \pm 0.02$ for the CTSYM, and $S^2 = 0.83 \pm 0.05$ for the CTSYMTOTO deoxyribose spins were found. The S^2 values for the 5′-terminal deoxyribose are lower than for the other residues. The DNA backbone in CTSYMTOTO is distorted and elongated at the site of intercalation, and the C3′ atom of the C3 deoxyribose residue has a very low $S^2 = 0.57 \pm 0.06$. The low order for this spin is interpreted in terms of exchange between the C2′-endo and O1′-endo conformations of the C3 deoxyribose. Significant chemical exchange processes were found for most of the aromatic spins in CTSYM that are interpreted in terms of microsecond to millisecond time scale dynamics. The microsecond to millisecond dynamics of the bases in CTSYM are quenched upon TOTO complex formation due to unwinding of the helix and an increase in the surface area of the bases in mutual contact and the large surface area in contact with the intercalated dye. The derived order parameters combined with the solution structure provide motional models for conformational changes induced in the backbone in response to the ligand binding.

Ligand binding to DNA is one of the fundamental processes of DNA metabolism in which the ligands often show remarkable sequence selectivity. However, the detailed molecular interactions that give rise to this sequence-selective binding are often unclear. Specific hydrogen bonding, shape complementarity, and electrostatics are some of the interactions that are invoked to account for DNA−ligand sequence specificity. Intercalation is a relatively nonspecific interaction that involves the insertion of all or part of the ligand between adjacent base pairs accompanied by distortions in the sugar phosphate backbone and unwinding of the DNA helix. Intercalators associate with DNA primarily through nonspecific π stacking interactions. The homodimeric dye TOTO (Figure 1) binds to DNA via bis-intercalation preferentially at the 5′-CTAG-3′ or the 5′-CCGG-3′ sequences forming stable, highly fluorescent complexes with double-stranded DNA (dsDNA)[1] that are useful in the nonradioactive detection of DNA fragments (*1*, *2*). The TOTO−DNA complex represents the prototypical interaction of an intercalator with

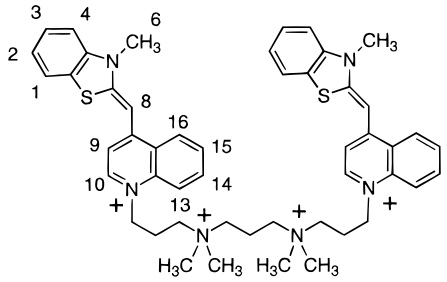

FIGURE 1: Structures of TOTO indicating the numbering scheme.

DNA and provides an excellent system in which to examine some of the structural aspects of DNA−ligand interactions. A general problem in the study of the interaction of ligands with DNA is determining the sources of intermolecular affinity and specificity. The changes in conformational

† This work was supported in part by American Cancer Society grant IN-163, the Kentucky Medical Center Research Fund (831) and Kentucky-NSF EPSCoR Program (EPS-9452895).

* Corresponding author e-mail, hps@pop.uky.edu; phone, (606) 257-4790; fax, (606) 257-8940.

[1] Abbreviations: dsDNA, double stranded DNA; EDTA, ethylenediamine tetraacetic acid; NMR, nuclear magnetic resonance; NOE, nuclear Overhauser effect; NOESY, nuclear Overhauser effect spectroscopy; COSY, correlation spectroscopy; DQF−COSY, double quantum filtered correlation spectroscopy; DEPT, distotionless enhancement by polarization transfer; HMQC, heteronuclear multiple quantum coherence; TOCSY, total correlated spectroscopy; RMD, restrained molecular dynamics; ppm, parts per million.

10.1021/bi980789e CCC: $15.00
Published on Web 11/12/1998

freedom associated with complex formation are expected to substantially impact both the binding specificity and affinity of the DNA−ligand complex. A complete understanding of DNA structure must therefore include a quantitative description of dynamics both in the normal nucleic acid and in DNA−ligand complexes. Several studies have shown that DNA exhibits sequence-dependent structural and conformational polymorphism in solution and that these conformational equilibria may play a significant role in the interaction of DNA with specific proteins and small molecule ligands. Consequently, it is important to describe the internal motions of the DNA and DNA−ligand complexes to more completely understand the interactions of DNA-specific drugs.

NMR is uniquely useful among the experimental techniques used to characterize internal motions in nucleic acids because a large number on nuclear sites within a given molecule can be simultaneously studied over a wide range of time scales (*3*). For example, information about fast internal motions and overall rotational tumbling of a molecule in solution can be obtained from ^{13}C NMR relaxation measurements. These measurements are difficult to achieve directly because of crowding in the spectra of biological macromolecules and the low natural abundance (1.1%) and decreased sensitivity of ^{13}C nuclei ($^1/_4$ that of protons). The introduction of two-dimensional proton-detected heteronuclear techniques has reduced some of the problems resulting from the inherent lack of sensitivity of ^{13}C nuclei and the limited resolution of one-dimensional NMR techniques (reviewed by Bax et al., ref *4*). Recently, investigations of NMR relaxation have been carried out for ^{13}C nuclei at natural abundance by indirect detection in various proteins (*5*−*9*) for psoralen-damaged DNA (*10*), and by direct carbon detection for some DNA oligomers (*11*). Selective ^{13}C labels have been incorporated into DNA oligomers at the C1′ position, and their relaxation and dynamic behavior have been measured (*12*). NMR relaxation experiments can provide a wealth of information on both the structure and conformational equilibria of DNA in solution, and several studies have attempted to describe the internal motions of the DNA backbone (*13*−*16*), of sugar repuckering (*11, 16*), and of base-pair opening (*17*−*19*). Precise conclusions were difficult to deduce from these studies because there are usually several motions taking place simultaneously with different amplitudes and on different time scales extending from picosecond to second. Additionally, the correlations between atomic motion and nucleic acid function are not completely understood.

The structure of TOTO complexed with the DNA oligomer $d(CGCTAGCG)_2$ has been determined by NMR spectroscopy and restrained molecular dynamics (Figure 4b,d) (*20*). The binding of TOTO to dsDNA results in substantial structural distortion to the normal B-form DNA helix. The three-dimensional structure of the complex shows that the conformational differences between undamaged DNA and the complex result in an unwinding of the helix of 60° with an overall helical repeat of 12 base pairs. The largest structural distortions are localized to the four-base-pair binding site, and the DNA structure outside the binding site returns to normal B-form conformation. In contrast to other intercalators, the sequence selectivity of TOTO arises from the interaction of the intercalated chromophores with the bases, apparently due to the ability of the TOTO chromophore to adapt to the propeller twist of the bases in the 5′-CT-3′ step (*20*). The cationic linker of TOTO contributes significantly to the binding strength of the dye to DNA, but it appears to be a spectator with respect to the sequence selectivity.

Table 1: Proton and Carbon Chemical Shifts of CTSYM at 298 K

	C1	G2	C3	T4	A5	G6	C7	G8
				Proton Chemical Shifts[a]				
H1′	5.75	5.96	5.97	5.58	6.03	5.70	5.75	6.13
H3′	4.70	5.00	4.77	4.87	5.05	4.96	4.78	4.66
H4′	4.07	4.38	4.24	4.14	4.41	4.37	4.14	4.16
H5/H2	5.85		5.38		7.39		5.32	
H8/H6	7.61	7.98	7.43	7.40	8.22	7.69	7.28	7.90
				Carbon Chemical Shifts[b]				
C1′	88.59	84.95	87.22	86.01	85.26	84.4	86.96	85.19
C3′	78.18	80.42	77.51	78.46	80.04	78.73	77.09	73.88
C4′	88.66	87.88	86.09	86.07	87.93	87.2	86.38	88.39
C5/C2	99.88		98.88		154.52		98.84	
C6/C8	143.67	138.72	142.92	140.22	142.32	137.78	143	139.55

[a] Measured relative to the HOD signal at 4.78 ppm referenced to DSS (0 ppm). [b] The carbon frequency was referenced indirectly to DSS relative to the HOD signal at 4.78 ppm.

Table 2: Proton and Carbon Chemical Shifts of CTSYMTOTO at 298 K

	C1	G2	C3	T4	A5	G6	C7	G8
				Proton Chemical Shifts[a]				
H1′	5.65	5.64	5.95	4.77	5.35	5.82	5.69	6.08
H3′	4.62	4.84	4.59	4.63	5.11	4.88	4.78	4.65
H4′	4.01	4.23	4.05	4.06	4.27	4.56	4.16	4.15
H5/H2	5.75		4.50		7.05		5.30	
H8/H6	7.51	7.74	6.40	6.97	8.17	7.83	7.27	7.89
				Carbon Chemical Shifts[b]				
C1′	88.06	84.29	86.17	87.93	84.66	84.54	86.55	84.79
C3′	78.1	79.21	74.15	76.83	80.54	78.99	77.09	73.52
C4′	88.27	87.13	84.74	87.06	87.78	88.66	85.92	88.07
C5/C2	99.5		96.73		153.8		98.74	
C6/C8	143.27	138.1	141.43	140.09	141.66	137.29	142.52	139.28

Proton and Carbon Chemical Shifts[c]

atom	δ ^1H ppm	atom	δ ^1H ppm	atom	δ ^{13}C ppm	atom	δ ^{13}C ppm
H1	7.59	H10	7.99	C1	125.36	C10	145.62
H2	7.47	H13	7.13	C2	128.43	C13	117.64
H3	7.59	H14	7.01	C3	131.8	C14	134.69
H4	7.44	H15	6.67	C4	115.51	C15	127.53
H8	6.13	H16	7.36	C8	90.07	C16	126.52
H9	6.49			C9	110.93		

[a] Measured relative to the HOD signal at 4.78 ppm referenced to DSS (0 ppm). [b] The carbon frequency was referenced indirectly to DSS relative to the HOD signal at 4.78 ppm. [c] The proton values are measured relative to the HOD signal at 4.78 ppm referenced to DSS. The carbon frequency was referenced indirectly to DSS relative to the HOD signal at 4.78 ppm.

This paper reports on a study of the dynamics of the parent (CTSYM) and TOTO complex (CTSYMTOTO) of the DNA oligomer $d(CGCTAGCG)_2$ based on ^{13}C relaxation measurements made by using proton-detected ^{13}C-^1H 2D NMR spectroscopy. The data for the CTSYM (Table 1) and the CTSYMTOTO (Table 2) are compared with each other and with other relaxation data available for other DNA molecules. This study forms the basis for a comparative analysis with other types of drug−DNA complexes and covalent damage to DNA. These comparisons will provide detailed information on the changes in structure and dynamics that occur as a result of ligand binding to the DNA helix and will suggest mechanisms used for the regulation of DNA metabolism.

EXPERIMENTAL PROCEDURES

Materials. The CTSYMTOTO complex was prepared as described (*20*). The following numbering scheme is used to describe the residues in the CTSYM and CTSYMTOTO:

```
5'- C1 G2 C3 T4 A5 G6 C7 G8 -3'
3'- G8 C7 G6 A5 T4 C3 G2 C1 -5'
```

All measurements on the CTSYM and CTSYMTOTO were made on one 4 mM and on one 3 mM sample, respectively, in 99.9% D_2O adjusted to pH 7.0, 20 mM PO_4^-, 10 mM NaN_3, 100 mM NaCl, and 0.1 mM EDTA.

Structural Coordinates. The atomic coordinates and NOE-derived restraints for the CTSYMTOTO were obtained from PDB entry 108D (*20*). Models for the CTSYM were generated using standard Arnott parameters for B-form DNA in the *Biopolymer* module of *insightII* (v. 95.0.6) (Biosym Technologies, San Diego, CA). The 40 structures for the TOTO complex available in entry PDB 108D were re-analyzed with the program CURVES 3.1 to extract the sugar pseudorotation parameters and the backbone torsional angles (*21, 22*). The results are presented in Table 5.

Acquisition of NMR Spectra. Experiments were recorded at 298 K on a Varian Inova 500 (11.74 T) spectrometer. The ^{13}C spin−lattice (R_1) and spin−spin (R_2) relaxation rate constants and steady-state {^1H}-^{13}C NOEs were measured from ^1H-detected ^1H-^{13}C correlation spectra as previously described (*6, 9, 10*). ^1H-^{31}P HSQC spectra were acquired as previously described (*23*).

All relaxation spectra were recorded with a spectral width of 4489.3 Hz and 1024 real points in ω_2; digital oversampling by a factor of 40 was employed to reduce baseline distortions associated with the spectrometer's low-pass filters (*24*), and all experiments were recorded using the hypercomplex method of phase incrementation to obtain quadrature phase detection in ω_1 (*25*). A spectral width of 2700 Hz was used in ω_1 that led to extensive folding of the spectrum (*26*), and 64 complex points were collected as previously described (*10*). For the R_1 and R_2 measurements the relaxation delays in the pulse sequences were set to 3.4 s (approximately 1.9 times the average ^1H spin−lattice relaxation time of 1.78 s, except for the CTSYM adenine H2 protons which had ^1H T_1 of 5.0 s) and the total numbers of transients recorded per t_1 point were 256 and 512 for real and complex data, respectively. For the {^1H}-^{13}C NOE measurements the ^1H recovery period prior to acquisition was 4.0 s (greater than eight times the longest ^{13}C spin−lattice relaxation time) and the total numbers of transients recorded per t_1 point were 1024 and 2048 for real and complex data, respectively.

Two spectra, one with and one without ^1H saturation, were recorded in an interleaved manner to yield heteronuclear steady-state {^1H}-^{13}C NOEs which were acquired over a 12 day period. To measure R_1, nine experiments with relaxation delays T of 0.01, 0.038, 0.073, 0.143, 0.213, 0.423, 0.633, 0.948, and 1.893 s were recorded in an interleaved manner over a 13 day period. Monoexponential evolution of carbon magnetization was obtained by saturation of the protons by applying π pulses every 7 ms during the recovery delay in the T_1 experiments (*9*). T_2 experiments were performed with a Carr-Purcell-Meiboom-Gill (CPMG) spin−echo sequence with nine transverse relaxation delays T of 1, 5, 10, 15, 20, 30, 40, 50, and 60 ms in an interleaved manner over a 13 day period. The CPMG sequence was not modified to suppress the effects of cross-correlation between dipolar and chemical shift anisotropy (CSA) relaxation mechanisms (*27*).

Data Processing. Felix (Biosym, San Diego) was used for data processing. A cosine bell function was applied to the first 512 complex data points in each ω_2 FID. Prior to Fourier transformation the data were zero-filled once. In ω_1, the interferogram was extended to 128 complex points by linear prediction, followed by multiplication with a cosine bell function.

Analysis of Relaxation Rate Constants and NOEs. Intensities of the resonance peaks in the two-dimensional spectra were determined as peak heights. The uncertainties in the measured peak heights (σ_h) were taken to be the rmsd baseplane noise in the spectra. These values are generally underestimated in comparison with those obtained from duplicate data points. However, the limitations imposed by the use of ^{13}C at natural abundance precluded the acquisition of replicate measurements. The relaxation rate constants R_1 and R_2 and uncertainties were obtained from nonlinear least-squares fitting of monoexponential equations for longitudinal and transverse relaxation as described (*6, 10*).

Calculation of Model-Free Parameters. The relaxation of a methine ^{13}C nucleus at natural abundance at high field strengths is dominated by the dipolar interaction with the directly attached proton and by the CSA mechanism (*28*). The ^{13}C R_1 and R_2 relaxation rate constants and the NOEs are given by the following:

$$R_1 = (d^2/4)[J(\omega_H - \omega_C) + 3J(\omega_C) + 6J(\omega_H + \omega_C)] + c^2 J(\omega_C) \quad (1)$$

$$R_2 = (d^2/8)[4J(0) + J(\omega_H - \omega_C) + 3J(\omega_C) + 6J(\omega_H) + 6J(\omega_H + \omega_C)] + (c^2/6)[3J(\omega_C) + 4J(0)] + R_{ex} \quad (2)$$

$$\mathrm{NOE} = 1 + (d^2/4R_1)(\gamma_H/\gamma_C)[6J(\omega_H + \omega_C) - J(\omega_H - \omega_C)] \quad (3)$$

in which

$$d = (\mu_0 h/8\pi^2)\gamma_H\gamma_C(1/r_{CH}^3) \quad (4)$$

$$c = \omega_C(\sigma_{para} - \sigma_{perp})/\sqrt{3} \quad (5)$$

and μ_0 is the permeability of free space, h is Plank's constant, γ_H and γ_C are the gyromagnetic ratios of ^1H and ^{13}C, respectively, r_{CH} is the carbon−proton bond length (1.09 Å), ω_H and ω_C are the Larmor frequencies of ^1H and ^{13}C, and σ_{para} and σ_{perp} are parallel and perpendicular components of the chemical shift tensor. The estimated CSA for an sp^3 hybridized C1′ carbon is 41 ppm, while the estimated CSA for an sp^2 aromatic carbon is 185 ppm (*12, 29*).

The amplitudes and time scales of intramolecular motions of individual C−H bond vectors for the CTSYM and CTSYMTOTO were obtained by fitting the observed relaxation data to the extended Lipari and Szabo model-free formalism of the spectral density function (*6, 30*−*32*). In this approach the spectral density function is modeled as

$$J(\omega) = \frac{2}{5}\left[\frac{S^2\tau_m}{1+(\omega\tau_m)^2} + \frac{(1-S^2_f)\tau'_f}{1+(\omega\tau'_f)^2} + \frac{(S^2_s - S^2)\tau'_s}{1+(\omega\tau'_s)^2}\right] \quad (6)$$

where $\tau'_f = \tau_f\tau_m/(\tau_f + \tau_m)$, $\tau'_s = \tau_s\tau_m/(\tau_s + \tau_m)$, τ_m is the overall rotational correlation time of the molecule, τ_f is the effective correlation time for internal motions on a fast time scale ($\tau_f < 100-300$ ps), τ_s is the effective correlation time for internal motions on a slow time scale ($\tau_f < \tau_s < \tau_m$), $S^2 = S^2_fS^2_s$ is the square of the generalized order parameter characterizing the amplitude of the internal motions, and S^2_f and S^2_s are the squares of the order parameters for the internal motions on the fast and slow time scales, respectively. Motions represented by S^2 refer to internal dynamics on the picosecond to nanosecond time scale. The effective correlation (either τ_f or τ_s) depends on the rate of motion of the C−H bond vector with the value ranging from 0 for isotropic internal motion to unity for completely restricted motion. The R_{ex} term of eq 2 represents conformational exchange and other pseudo-first-order processes on a time scale much slower than the overall rotational correlation time (τ_m) that contribute to the decay of transverse magnetization (*33*). Because the delay in the CPMG sequence used to measure R_2 is 1 ms, exchange processes will only contribute to this relaxation if the microscopic exchange rate is within approximately an order of magnitude of 1000 s^{-1}. These processes are undetectable if the resonance frequency difference between the conformers contributing to the process approaches 0. Thus, conformational exchange processes represented by R_{ex} will be referred to as dynamics on a microsecond to millisecond time scale. Fitting experimental data using eq 6 requires a maximum of six free parameters, the five parameters in the equation and the chemical exchange term R_{ex} in eq 2. Mandel et al. describe five simpler dynamic models derived from eq 6 that contain an overall correlation time, a maximum of three internal motional parameters, and a single internal time scale parameter, either τ_f or τ_s (*34*). The five models consist of the following subsets of the extended model-free parameters in eq 6: (1) S^2; (2) S^2, τ_f; (3) S^2, R_{ex}; (4) S^2, τ_f, R_{ex}; (5) S^2_s, S^2_f, τ_s. Model 1 is appropriate if motions on the slow time scale are negligible and motions on the fast time scale are very fast (<20 ps). Model 2 is the original formulation of Lipari and Szabo (*30*) and is applicable if motions on the slow time scale are negligible. Models 3 and 4 are derived from models 1 and 2, respectively, by including a nonzero chemical exchange contribution, R_{ex}, in the relaxation model. For models 1−4, $S^2 = S^2_f$. Model 5 assumes only that $\tau_f \rightarrow 0$. We fit the three relaxation data for each spin (R_1, R_2, and NOE) to each of the five models using the program ModelFree (version 3.1) (*6*). Selection of the most appropriate model to describe the data for each spin is described in detail in Mandel et al. (*34*). The quality of the model selection and fitting was assesed by examining the residual sum square error for each spin. For model 1, the $\alpha = 0.05$ critical value is approximately $\Gamma = 6.0$; for models 2 and 3, $\alpha = 0.05$ is approximately $\Gamma = 3.8$; and for models 4 and 5, the residual sum square error is required to be 0.

Molecular Modeling. NOE-derived distance restraints were obtained from PDB entry 108D and were incorporated into an RMD procedure to test the conformational effect of various backbone torsion angles on the CTSYMTOTO complex. The RMD and energy minimization calculations were performed using Discover (v. 2.9.5) with modified AMBER force-field potentials. The models were displayed using insightII (v. 2.3.0) (Biosym Technologies, San Diego). The NOE-derived distance restraints and torsion restraint to be tested were applied to the CTSYMTOTO structure, and the model was energy-minimized. This was followed by 28 ps of restrained molecular dynamics at 600 K for 4 ps, followed by cooling to 200 K in 50 K steps of 3 ps each. The final structure was then energy-minimized to a maximum derivative of 0.01 Å.

The pseudo-energy term used to enforce the distance restraints was the following:

$$E_{constr} = k_1(r - r_2)^2 \text{ when } r_2 > r$$
$$= 0 \text{ when } r_3 \geq r \geq r_2$$
$$= k_2(r - r_3)^2 \text{ when } r_3 > r$$

where r_2 and r_3 are the upper and lower distance bounds determined from the cross-peak volumes and k_1 and k_2 are the force constants that could be independently adjusted for each restraint. An upper and lower bound force constant of 50 kcal/mol Å^2 was assigned for all NOE-derived distance restraints. An additional 22 distance restraints were included to enforce Watson−Crick hydrogen bonding throughout the calculations. Three hydrogen bonds were included for each of the six G−C base pairs and two hydrogen bonds for each of the A−T base pairs with lower and upper bounds of 1.7 and 2.1 Å, respectively. Helix parameters were calculated with the program CURVES 3.1 (*21*−*22*).

RESULTS

Carbon chemical shift assignments for the CTSYM and CTSYMTOTO were obtained by correlating the ^{1}H chemical shift values obtained from analysis of NOESY, TOCSY, and DQF−COSY spectra (*20*) with the ^{13}C chemical shifts from HMQC spectra. HMQC spectra of the CTSYMTOTO and CTSYM are shown in Figure 2. The relaxation parameters, R_1, R_2, and NOE were obtained by analysis of proton-detected natural abundance ^{13}C-^{1}H heteronuclear correlation spectra of the CTSYMTOTO and CTSYM. Signal-to-noise was calculated as the mean peak height in the 1 ms relaxation delay R_1 experiment, the 1 ms relaxation delay R_2 experiment, and the NOE experiment without proton saturation over the RMS baseline noise in each spectrum, respectively. Mean values for the signal-to-noise ratios in the spectra for the CTSYMTOTO were 32.7, 32.6, and 36.1 for R_1, R_2, and NOE measurements, respectively. For the CTSYM, the signal-to-noise ratios in the spectra were 101, 151, and 141 for R_1, R_2, and NOE measurements, respectively. Reliable quantitation of peak intensities for the CTSYM and CTSYMTOTO was possible for all methine carbons in the molecule (aromatic, C1′, C3′, and C4′) except for CTSYMTOTO G6C8 and C7C3′. Sample R_1 and R_2 relaxation decay curves are shown in Figure 3. In an independent study (to be reported elsewhere) the dynamics for a DNA decamer were determined and the issues of accuracy and precision in the relaxation data were examined. The R_1, R_2, and the NOE were determined for the decamer from multiple independent spectra with signal-to-noise values comparable to that for

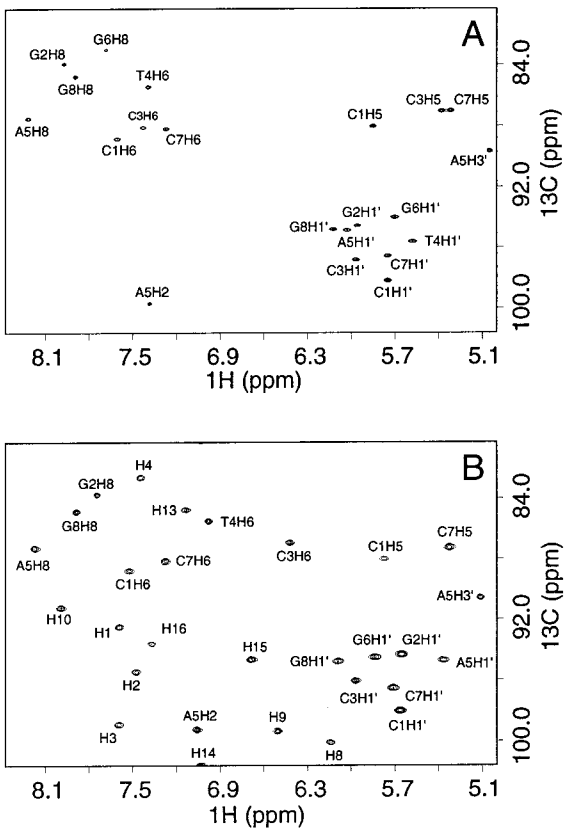

FIGURE 2: The aromatic and most of the deoxyribose C1′ portion of the ^{13}C-^{1}H correlation spectrum for (a) the CTSYM and (b) the CTSYMTOTO from the pulse sequence used to measure R_1 with a delay of 1 ms.

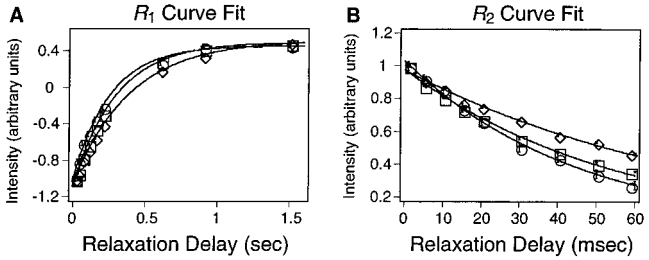

FIGURE 3: ^{13}C relaxation data for the CTSYM A5C8 (squares), CTSYM C3C1′ (diamonds), and CTSYMTOTO TOTO-C10 (circles): (A) R_1 relaxation decay curves; and (B) R_2 relaxation decay curves. The error bars are smaller than the size of the data symbols.

the CTSYMTOTO. Similar percent errors in the measurement of relaxation parameters were obtained for the decamer compared to the CTSYMTOTO.

Global Tumbling. Relaxation data were analyzed for isotropic overall rotational motion of both the CTSYMTOTO and CTSYM which assumes a spherical shape for the DNA oligomers in solution. Final optimization with the selected dynamic model for each nuclear spin gave a global τ_m of 3.44 ns for the CTSYM and a global τ_m of 3.48 ns for the CTSYMTOTO. Optimizations converged to the same result for initial estimates of τ_m from 2 to 5 ns. The 10% trimmed mean R_2/R_1 ratios (calculated by taking the R_2/R_1 ratio for all of the spins, calcualting the mean, comparing the mean to all of the ratios, and discarding the 10% spins furthest from the mean) for the CTSYM and CTSYMTOTO interpreted using the simple Lipari and Szabo formalism gave overall correlation times of 3.59 and 3.56 ns, respectively. The global τ_m calculated from the ^{13}C relaxation data compare favorably with the values that gave the best fit for the ^{1}H NOESY relaxation data that were converted to interproton distances using the RANDMARDI complete relaxation matrix analysis procedure used to determine the solution structure of the CTSYMTOTO (*10*, *20*, *35*). In that procedure, a τ_m of 3.75 ns for the CTSYMTOTO ^{1}H NOE data gave the best fit. The rotational correlation times calculated from the ^{13}C relaxation data are also longer than those estimated by either fluorescence for oligomers of similar size or the Stokes−Einstein−Debye model values (*36*). The discrepancies in τ_m values probably arise from a number of causes, including simplifying assumptions introduced for each model, and these estimates for the τ_m are in acceptable agreement.

Dynamic Parameters. Optimized values of the model-free parameters and the relaxation data are given in Table 3 for the CTSYM and Table 4 for the CTSYMTOTO. Order parameters are mapped onto the three-dimensional structure of the CTSYM and CTSYMTOTO in Figure 4, parts a and b, respectively, using a pseudo-color representation. Chemical exchange terms are mapped onto the three-dimensional structure of the CTSYM and CTSYMTOTO in Figure 4, parts c and d, respectively, using a pseudo-color representation. The order parameter (S^2) correlates with the semiangle θ of the "wobbling in a cone" model, according to $S^2 = [\cos\theta\,(1 + \cos\theta)/2]^2$ (*31*). Tables 3 and 4 list the semiangle of the cone using this simple diffusion model for the CTSYM and CTSYMTOTO.

The most striking feature for the order parameters is that they are quite high for both molecules despite the large structural distortions introduced by the bis-intercalation. The order parameters calculated indicate that the aromatic atoms in the CTSYM are highly constrained on the fast motion time scale with an average $S^2 = 0.79 \pm 0.02$. The least constrained spin was the terminal C1C5, and the most highly constrained spin was the T4C6 and C3C6 (Table 3). The DNA aromatic spins in the CTSYMTOTO had an almost identical average $S^2 = 0.80 \pm 0.04$ where the G8C8 was the least constrained and the C7C5 spin the most highly constrained (Table 2). There is no significant decrease in the average order parameter for these residues in the CTSYMTOTO (see Table 4 and Figure 4a,b).

The calculated order parameters indicate that the deoxyribose C1′ atoms in the CTSYM are highly constrained on the fast motion time scale with an average $S^2 = 0.76 \pm 0.02$. The S^2 for the C1′ spins are similar to, but have a wider range than, the aromatic atoms ranging from a low for C1C1′ to a high for G2C1′. The average for the deoxyribose spins in the CTSYMTOTO was $S^2 = 0.83 \pm 0.05$.

In general, the order parameters for the spins in the TOTO complex are somewhat higher than the corresponding spins in CTSYM. The most notable exception is C3C3′, which is discussed in greater detail below.

Interestingly, the S^2 values for the C1′, C3′, and C4′ deoxyribose spins in the various residues of the CTSYM are not related in any simple way and are shown graphically in Figure 5. There are clearly sequence context-dependent variations in the flexibility of the DNA. Sequence-dependent variation in the deoxyribose order parameters for the molecule d(GCGTACGC)$_2$ and other oligomers has been

Table 3: Base and Backbone Relaxation and Dynamic Parameters for CTSYM

atom	R_1 (s^{-1})	R_2 (s^{-1})	NOE	model[a]	S^2_{tot}	S^2_{slow}	S^2_{fast}	τ_f (ps)	R_{ex} (s^{-1})	Γ_i	θ
C1C6	3.52 ± 0.10	27.71 ± 4.00	1.21 ± 0.02	4	0.79 ± 0.02		0.79 ± 0.02	36 ± 10	9 ± 4	0.00	23°
C1C5	3.05 ± 0.04	30.00 ± 4.00	1.23 ± 0.02	4	0.67 ± 0.01		0.67 ± 0.01	26 ± 5	14 ± 4	0.00	29°
G2C8	3.43 ± 0.13	18.21 ± 0.54	1.21 ± 0.05	1	0.79 ± 0.02		0.79 ± 0.02			3.12	22°
C3C6	3.74 ± 0.10	32.65 ± 2.44	1.15 ± 0.03	3	0.88 ± 0.02		0.88 ± 0.02		12 ± 3	1.03	16°
C3C5	3.38 ± 0.10	25.00 ± 5.00	1.14 ± 0.02	1	0.80 ± 0.02		0.80 ± 0.02			2.45	22°
T4C6	3.83 ± 0.06	29.53 ± 2.68	1.18 ± 0.02	4	0.88 ± 0.02		0.88 ± 0.02	44 ± 17	9 ± 3	0.00	17°
A5C8	3.39 ± 0.09	28.24 ± 2.50	1.19 ± 0.03	4	0.77 ± 0.02		0.77 ± 0.02	23 ± 9	10 ± 3	0.00	24°
A5C2	3.44 ± 0.07	32.23 ± 3.61	1.12 ± 0.02	3	0.81 ± 0.02		0.81 ± 0.02		13 ± 4	0.00	21°
G6C8	3.32 ± 0.13	27.23 ± 5.42	1.14 ± 0.04	1	0.79 ± 0.03		0.79 ± 0.03			2.81	22°
C7C6	3.77 ± 0.12	34.64 ± 2.07	1.18 ± 0.03	4	0.86 ± 0.03		0.86 ± 0.03	39 ± 23	15 ± 2	0.00	18°
C7C5	3.30 ± 0.13	16.40 ± 1.31	1.20 ± 0.02	2	0.73 ± 0.03		0.73 ± 0.03	25 ± 7		0.44	26°
G8C8	3.18 ± 0.09	16.21 ± 0.40	1.16 ± 0.03	1	0.72 ± 0.01		0.72 ± 0.01			4.91	26°
C1C1′	2.06 ± 0.04	8.68 ± 0.20	1.61 ± 0.02	2	0.50 ± 0.01		0.50 ± 0.01	49 ± 2		0.06	38°
G2C1′	2.84 ± 0.10	14.15 ± 2.15	1.22 ± 0.03	1	0.91 ± 0.03		0.91 ± 0.03			4.27	14°
C3C1′	2.54 ± 0.09	12.72 ± 0.57	1.25 ± 0.02	2	0.77 ± 0.02		0.77 ± 0.02	24 ± 6		0.23	23°
T4C1′	2.59 ± 0.08	14.50 ± 1.55	1.30 ± 0.03	2	0.78 ± 0.03		0.78 ± 0.03	41 ± 9		0.87	23°
A5C1′	2.60 ± 0.16	17.57 ± 1.44	1.25 ± 0.02	4	0.80 ± 0.05		0.80 ± 0.05	29 ± 22	4 ± 2	0.00	22°
G6C1′	2.79 ± 0.06	12.72 ± 2.31	1.25 ± 0.02	2	0.86 ± 0.02		0.86 ± 0.02	42 ± 12		0.47	18°
C7C1′	2.53 ± 0.09	12.06 ± 0.68	1.38 ± 0.02	2	0.71 ± 0.02		0.71 ± 0.02	52 ± 8		0.02	27°
G8C1′	2.50 ± 0.07	14.10 ± 1.24	1.33 ± 0.02	2	0.75 ± 0.02		0.75 ± 0.02	41 ± 7		1.72	25°
C1C3′	2.10 ± 0.06	7.46 ± 1.21	1.76 ± 0.03	2	0.45 ± 0.02		0.45 ± 0.02	62 ± 4		0.33	40°
G2C3′	2.69 ± 0.07	13.64 ± 0.78	1.28 ± 0.02	2	0.81 ± 0.02		0.81 ± 0.02	43 ± 9		0.00	21°
C3C3′	2.49 ± 0.16	13.70 ± 1.05	1.36 ± 0.03	2	0.75 ± 0.04		0.75 ± 0.04	53 ± 15		1.42	25°
T4C3′	2.47 ± 0.06	11.58 ± 0.98	1.33 ± 0.03	2	0.72 ± 0.02		0.72 ± 0.02	38 ± 6		0.34	27°
A5C3′	2.64 ± 0.07	16.78 ± 0.92	1.22 ± 0.02	4	0.83 ± 0.02		0.83 ± 0.02	22 ± 8	3 ± 1	0.00	20°
G6C3′	2.84 ± 0.09	11.30 ± 0.77	1.34 ± 0.02	5	0.62 ± 0.05	0.81 ± 0.03	0.76 ± 0.06	66 ± 154		0.00	32°
C7C3′	2.39 ± 0.14	13.14 ± 1.56	1.43 ± 0.03	2	0.67 ± 0.03		0.67 ± 0.03	53 ± 11		1.28	29°
G8C3′	1.96 ± 0.06	10.66 ± 0.96	1.58 ± 0.02	4	0.49 ± 0.02		0.49 ± 0.02	42 ± 3	2 ± 1	0.00	39°
C1C4′	2.25 ± 0.05	19.73 ± 1.70	1.57 ± 0.03	4	0.56 ± 0.02		0.56 ± 0.02	56 ± 4	10 ± 2	0.00	35°
G2C4′	2.62 ± 0.10	13.85 ± 0.53	1.36 ± 0.02	2	0.78 ± 0.02		0.78 ± 0.02	67 ± 12		2.40	23°
C3C4′	2.69 ± 0.10	16.47 ± 1.68	1.31 ± 0.02	2	0.81 ± 0.03		0.81 ± 0.03	55 ± 15		2.96	21°
T4C4′	2.57 ± 0.14	16.99 ± 1.77	1.29 ± 0.02	2	0.81 ± 0.04		0.81 ± 0.04	41 ± 19		4.42	21°
A5C4′	2.65 ± 0.09	15.27 ± 0.57	1.31 ± 0.02	4	0.79 ± 0.03		0.79 ± 0.03	48 ± 11	2 ± 1	0.00	23°
G6C4′	2.79 ± 0.08	13.01 ± 0.57	1.36 ± 0.02	2	0.79 ± 0.02		0.79 ± 0.02	73 ± 13		0.55	23°
C7C4′	2.77 ± 0.10	17.26 ± 1.44	1.28 ± 0.03	2	0.86 ± 0.03		0.86 ± 0.03	58 ± 32		4.33	18°
G8C4′	2.53 ± 0.08	25.73 ± 11.93	1.46 ± 0.02	2	0.68 ± 0.02		0.68 ± 0.02	64 ± 8		1.38	28°

[a] Dynamic models employed to fit the relaxation data for each nuclear spin as described in text and Mandel et al. (1995).

observed (*10*, *11*). These observations are consistent with the idea that microheterogeneity in the dynamics of DNA may correlate with structure. Comparison of the order parameters for the C1′, C3′, and C4′ spins in the CTSYM and the CTSYMTOTO reveals an interesting pattern. The S^2 values for the aromatic C1′ and C4′ spins are remarkably similar when compared between the two molecules while there are significant variations for the C3′ spins.

The CTSYM G6C3′ has a significantly lower S^2 when compared to the other CTSYM C3′ carbons and relative to the G6C1′ and G6C4′ atoms. This is an indication of significant conformational freedom for the CTSYM G6C3′ atom that is not available to the G6C1′ or G6C4′ atoms in the same sugar ring. The G6C3′ is connected through the five-bond C3′−O3′−P−O5′−C5′−C4′ backbone linkage to C7 corresponding to the five backbone bond angles G6 ϵ, G6 ζ, C7 α, C7 β, and C7 γ. This linkage is outside of the TOTO intercalation site, and C7 follows the purine−purine step composed of the A5-G6. Steric crowding at the A5-G6 step may alter the C7 stacking geometry and may allow the backbone between G6 and C7 to adopt multiple conformations. This is reflected in the conformational freedom at the CTSYM G6C3′ atom. S^2 values for the CTSYM C3, T4, and A5 sugar spins are uniformly high (Figure 5a).

The TOTO intercalation site is defined by the C3-G6 and T4-A5 base pairs. The quinolinium part of the thiazole orange chromophore is stacked between the two purine bases, and the benzothiazole part of the chromophore is between the two pyrimidine bases. The aliphatic amino linker chain connecting the two quinoline rings of TOTO lies in the minor groove of the complex. There are normal Watson−Crick interactions for all of the base pairs in CTSYMTOTO. The DNA backbone conformation on the purine side of the intercalation site is structurally different from that on the pyrimidine side (Table 5, Figure 4b,d). To accommodate the intercalation of the chromophore, the backbone linkage connecting the adjacent residues must adopt a more extended conformation than that found in B-form DNA. In the 5′-CT-3′ step, T4 γ opens from +*syn*-clinical (+*sc*, $\gamma = 36°$) to the *anti*-periplanar (*ap*, $\gamma = 180°$) conformation and the T4 α opens from −*syn*-clinical (−*sc*, $\alpha = -46°$) to the *ap* conformation while the T4 phosphate maintains a B-form like B_I conformation ($\epsilon = 155°$, $\zeta = -96°$). In the opposing 5′-AG-3′ step, the G6 phosphate adopts a more B_{II}-like conformation ($\epsilon = -58°$, $\zeta = 174°$). The dynamic behavior of the two sides of the intercalation site also shows differences. These backbone angles were calculated from structures derived from NOE restraints only. However, the torsions described for the phosphates are supported by the ^{31}P chemical shifts (vide infra).

The motions of the CTSYMTOTO G6 sugar atoms are much more restricted than the corresponding spins in CTSYM as evidenced by uniform, high order parameters. The A5-G6 purine side of the intercalation site is much more highly ordered than the C3-T4 pyrimidine side. The glycosidic torsion angles χ for both the A5 ($\chi = -80 \pm 3°$) and

Table 4: Base and Backbone Relaxation and Dynamic Parameters for CTSYMTOTO

atom	R_1 (s^{-1})	R_2 (s^{-1})	NOE	model[a]	S^2	τ_f (ps)	R_{ex} (s^{-1})	Γ_i	θ
C1C6	3.23 ± 0.24	22.48 ± 2.67	1.28 ± 0.10	1	0.82 ± 0.05			4.06	21°
C1C5	3.51 ± 0.34	21.05 ± 3.39	1.27 ± 0.13	1	0.86 ± 0.07			1.46	18°
G2C8	3.35 ± 0.26	18.59 ± 2.97	1.08 ± 0.10	1	0.81 ± 0.06			0.27	22°
C3C6	3.32 ± 0.22	22.27 ± 1.42	1.08 ± 0.07	1	0.86 ± 0.04			3.26	18°
C3C5	3.24 ± 0.18	20.89 ± 1.10	1.16 ± 0.09	1	0.83 ± 0.03			2.34	20°
T4C6	3.39 ± 0.20	18.77 ± 1.29	1.32 ± 0.09	1	0.81 ± 0.04			4.99	22°
A5C8	3.15 ± 0.17	20.15 ± 1.63	1.10 ± 0.07	1	0.79 ± 0.04			1.26	23°
A5C2	3.18 ± 0.15	18.61 ± 1.33	1.09 ± 0.05	1	0.77 ± 0.03			0.52	23°
C7C6	3.64 ± 0.20	20.85 ± 1.50	1.18 ± 0.07	1	0.88 ± 0.04			0.76	17°
C7C5	3.18 ± 0.17	21.92 ± 3.58	1.10 ± 0.05	1	0.78 ± 0.04			1.26	23°
G8C8	2.83 ± 0.18	18.93 ± 1.25	1.38 ± 0.09	4	0.57 ± 0.05	45 ± 16	5 ± 2	0.00	34°
C1C1′	2.02 ± 0.10	9.86 ± 1.21	1.48 ± 0.08	2	0.56 ± 0.04	37 ± 8		0.01	35°
G2C1′	2.80 ± 0.15	15.27 ± 1.31	1.28 ± 0.07	1	0.92 ± 0.04			3.00	14°
C3C1′	2.71 ± 0.17	12.28 ± 1.77	1.23 ± 0.06	1	0.86 ± 0.05			3.24	18°
T4C1′	2.61 ± 0.20	15.59 ± 5.04	1.35 ± 0.10	1	0.86 ± 0.06			3.70	18°
A5C1′	2.67 ± 0.20	17.63 ± 2.84	1.19 ± 0.08	1	0.90 ± 0.06			0.85	15°
G6C1′	2.87 ± 0.19	14.60 ± 2.48	1.29 ± 0.09	1	0.93 ± 0.05			2.12	12°
C7C1′	2.47 ± 0.13	13.60 ± 1.48	1.32 ± 0.08	1	0.81 ± 0.04			3.54	21°
G8C1′	2.42 ± 0.17	14.15 ± 3.28	1.31 ± 0.09	1	0.80 ± 0.05			2.68	22°
C1C3′	2.06 ± 0.10	9.17 ± 2.10	1.85 ± 0.10	2	0.42 ± 0.04	67 ± 9		0.36	42°
G2C3′	2.64 ± 0.14	19.38 ± 3.56	1.18 ± 0.05	1	0.88 ± 0.05			1.67	16°
C3C3′	2.13 ± 0.21	11.23 ± 2.95	1.52 ± 0.09	2	0.57 ± 0.06	47 ± 14		0.15	34°
T4C3′	2.72 ± 0.15	15.13 ± 3.44	1.33 ± 0.06	2	0.82 ± 0.05	67 ± 35		0.08	21°
A5C3′	2.88 ± 0.21	23.40 ± 1.69	1.15 ± 0.08	3	0.95 ± 0.05		7 ± 2	0.06	10°
G6C3′	2.78 ± 0.17	19.18 ± 2.53	1.23 ± 0.06	1	0.94 ± 0.05			2.79	11°
G8C3′	1.97 ± 0.08	7.56 ± 1.76	1.54 ± 0.06	2	0.51 ± 0.03	41 ± 6		0.74	37°
C1C4′	1.94 ± 0.08	11.52 ± 0.73	1.51 ± 0.06	4	0.52 ± 0.03	36 ± 6	2 ±1	0.00	37°
G2C4′	2.65 ± 0.11	12.79 ± 1.62	1.31 ± 0.04	2	0.80 ± 0.04	51 ± 18		0.36	22°
C3C4′	2.53 ± 0.15	16.23 ± 2.05	1.30 ± 0.07	1	0.85 ± 0.05			4.39	19°
T4C4′	2.69 ± 0.12	15.19 ± 1.41	1.30 ± 0.06	1	0.89 ± 0.04			4.59	16°
A5C4′	2.83 ± 0.14	14.12 ± 0.68	1.24 ± 0.05	1	0.88 ± 0.03			4.87	17°
G6C4′	2.63 ± 0.20	13.49 ± 1.46	1.29 ± 0.07	1	0.84 ± 0.05			3.20	19°
C7C4′	2.42 ± 0.13	16.84 ± 3.65	1.30 ± 0.05	2	0.75 ± 0.04	33 ± 12		1.25	25°
G8C4′	2.44 ± 0.08	12.18 ± 0.80	1.41 ± 0.05	2	0.70 ± 0.03	52 ± 10		0.00	28°
TOTOC1	3.34 ± 0.23	17.33 ± 1.55	1.16 ± 0.08	1	0.78 ± 0.04			1.07	23°
TOTOC2	3.60 ± 0.26	21.65 ± 2.68	1.07 ± 0.07	1	0.88 ± 0.06			0.69	17°
TOTOC3	3.55 ± 0.25	17.38 ± 1.80	1.07 ± 0.07	1	0.81 ± 0.04			2.29	21°
TOTOC4	3.47 ± 0.23	17.35 ± 3.15	1.09 ± 0.07	1	0.82 ± 0.05			0.87	20°
TOTOC8	3.38 ± 0.23	18.01 ± 1.20	1.07 ± 0.08	1	0.79 ± 0.04			1.23	23°
TOTOC9	3.22 ± 0.18	19.95 ± 1.88	1.11 ± 0.06	1	0.79 ± 0.04			0.46	22°
TOTOC10	4.00 ± 0.26	22.07 ± 0.92	1.03 ± 0.08	1	0.94 ± 0.03			1.76	12°
TOTOC13	3.27 ± 0.29	20.73 ± 2.91	1.29 ± 0.11	1	0.81 ± 0.06			2.83	21°
TOTOC14	3.74 ± 0.25	20.56 ± 1.80	1.16 ± 0.08	1	0.89 ± 0.05			0.35	16°
TOTOC15	3.65 ± 0.23	21.19 ± 2.19	1.22 ± 0.09	1	0.89 ± 0.05			1.32	16°
TOTOC16	3.52 ± 0.32	19.29 ± 3.31	1.01 ± 0.09	1	0.84 ± 0.07			1.81	19°

[a] Dynamic models employed to fit the relaxation data for each nuclear spin as described in text and Mandel et al. (1995).

the G6 ($\chi = -66 \pm 3°$) are at the edge of the range allowed for purines, which is well outside the normal range found in typical B-form and A-form structures (*37*). This results from the steric interaction between the deoxyribose C2′ methylene and the H8 of the purine. This interaction effectively pins the sugar residues of A5 and G6 into a single conformation of C2′-endo. The purity of a single conformation for both of the sugars is shown by the very high order parameters for their C1′, C3′, and C4′ atoms. The order parameters for the A5 and G6 deoxyribose are significantly higher than the already high values of the parent CTSYM DNA. Structurally, this can be rationalized by the quinolinium moiety of the chromophore being packed tighter against the helix backbone than the benzothiazole unit. This is a result of the linker chain placing the rear edge of the quinoline ring of the chromophore further into the minor groove than the benzothiazole rings are. The coplanar stacking of the A5-quinoline-G6 aromatic systems forces the alkyl chain connected to N11 of the thiazole orange to be jammed up against the A5 deoxyribose. The significant steric contacts of the bulky alkyl amino linker with the A5 deoxyribose also displace the A5 base into the major groove relative to the G6 base. As described above, the A5-G6 backbone is somewhat more compact than the more fully extended conformation of the C3-T4 side of the step.

The glycosidic torsion angle χ for both the CTSYMTOTO C3 and T4 are in the normal B-form DNA range of $\chi = -129 \pm 14°$. The DNA backbone between the two pyrimidines responds to the intercalation of the TOTO chromophore by allowing the T4 α and T4 γ torsion angles to adopt fully extended *anti*-periplanar (*ap*) conformations. If the T4 γ torsion angle were in the normal $+sc$ conformation, then there would not be enough room for the benzothiazole moiety because the C3 base would be rotated into the major groove over the chromophore making the A5-G6 backbone even more cramped. Since the A5 and G6 purine bases are already pegged against their deoxyribose C2′ methylenes and the quinoline ring is already in close van der Waals contact with the backbone, it is not possible to achieve this conformation. Rather, the backbone on the purine side of the intercalation site extends to accommodate the chromophore by allowing the A5 ζ torsion angle to adopt a fully

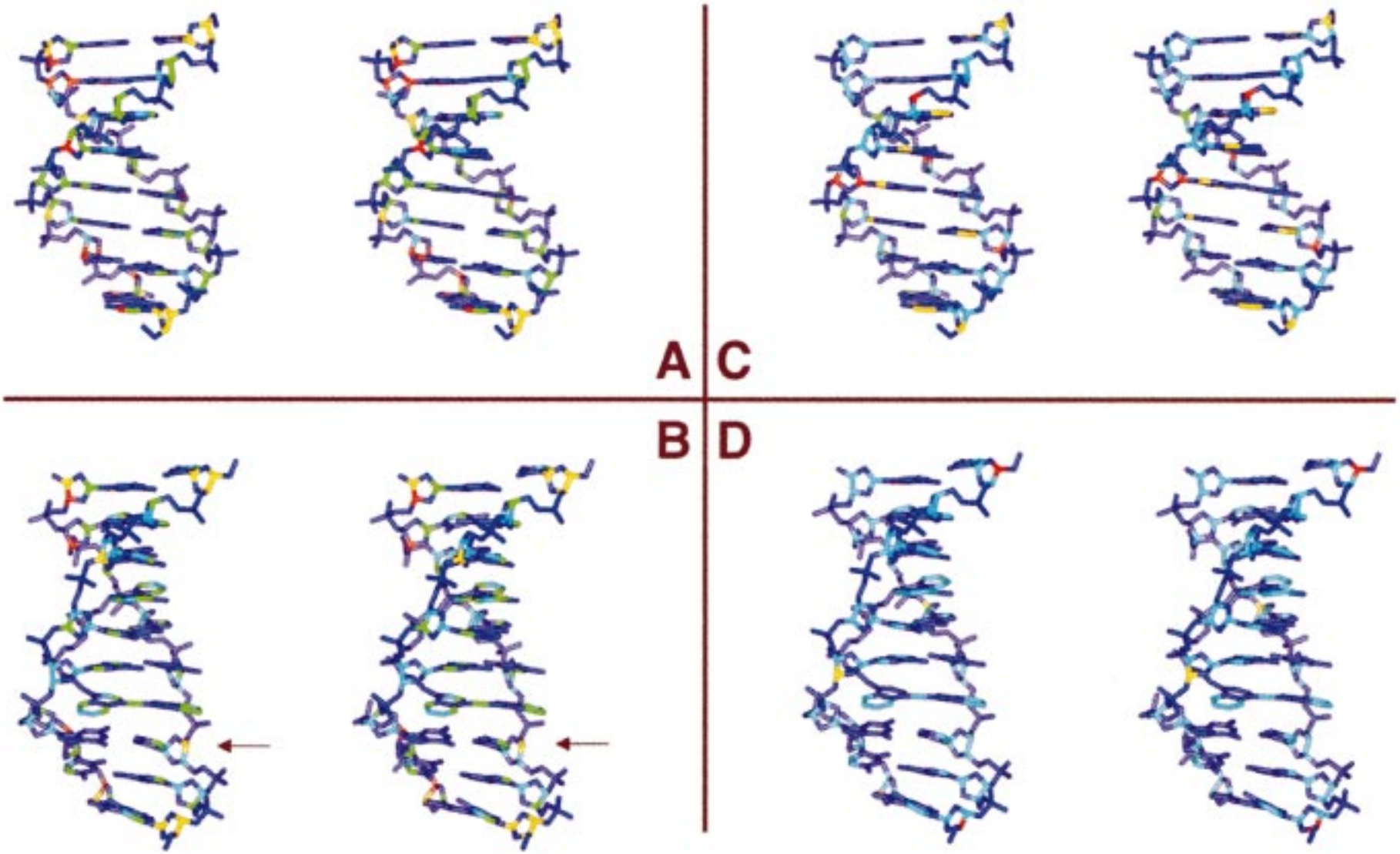

FIGURE 4: (a) Stereoview of the CTSYM color-coded by the value of the generalized order parameter. The structural coordinates were obtained from canonical B-form coordinates. (b) Stereoview of the CTSYMTOTO color-coded by the value of the generalized order parameter. Residue C3 is indicated. The structural coordinates were obtained from PDB entry 108D (*20*). The color scheme for (a) and (b) is blue, S^2 not determined; cyan, $S^2 \geq 0.85$; green, $0.85 \geq S^2 = 0.75$; red, $0.75 \geq S^2 \geq 0.65$; and yellow, $S^2 \geq 0.65$. (c) Stereoview of the CTSYM color-coded by the value of the chemical exchange term, R_{ex}. (d) Stereoview of the CTSYMTOTO color-coded by the value of the chemical exchange term, R_{ex}. The color scheme for (c) and (d) is blue, R_{ex} not determined; cyan, $R_{ex} = 0.0\ s^{-1}$; red, $0.0 > R_{ex} > 6.0$; and yellow, $R_{ex} > 6.0$. Atoms for which there is a S^2_{slow} are colored green. The protons have been omitted for clarity.

Table 5: Backbone Angles for CTSYMTOTO (TOTO Complex with d(CGCTAGCG)$_2$) Calculated from 40 NOE-Derived Structures (PDB 108D)[a]

torsions	χ C1′-N	ζ O3′-P	α P-O5′	β O5′-C5′	γ C5′-C4′	δ C4′-C3′	ϵ C3′-O3′	phase angle	pucker amplitude
C1	-158 ± 3					128 ± 2	-175 ± 1	134 ± 3	35 ± 1
G2	-103 ± 3	-79 ± 1	-51 ± 1	-151 ± 4	36 ± 5	148 ± 1	175 ± 1	161 ± 3	41 ± 1
C3	-143 ± 2	-90 ± 1	-68 ± 1	178 ± 2	46 ± 2	106 ± 1	-164 ± 6	103 ± 1	44 ± 0
T4	-116 ± 4	-88 ± 36	-175 ± 6	175 ± 18	-150 ± 2	120 ± 11	-174 ± 5	119 ± 13	42 ± 1
A5	-80 ± 5	-93 ± 5	-78 ± 7	-175 ± 5	45 ± 7	147 ± 3	-91 ± 21	157 ± 5	40 ± 2
G6 1	-63 ± 2	-174 ± 8	-9 ± 15	-168 ± 5	-53 ± 1	165 ± 3	-58 ± 5	167 ± 5	38 ± 5
G6 2	-66 ± 2	-174 ± 3	-10 ± 12	-167 ± 4	-51 ± 1	143 ± 2	139 ± 2	167 ± 5	38 ± 5
C7 1	-101 ± 1	126 ± 2	-88 ± 2	153 ± 2	39 ± 1	134 ± 1	-175 ± 0	143 ± 5	50 ± 1
C7 2	-107 ± 1	-86 ± 4	-59 ± 2	-178 ± 2	60 ± 1	142 ± 1	-175 ± 1	143 ± 5	50 ± 1
G8	-119 ± 3	-133 ± 1	47 ± 4	132 ± 5	-65 ± 1	98 ± 1		67 ± 1	43 ± 1
B-form	-129 ± 14	-96	-46	-146	36	156	155	162	38
A-form	-159 ± 21	-47	-75	-152	45	83	178	18	38

[a] Two distinct populations of conformers for the G6-pC7 and C7-pG8 base steps were found for backbone angles calculated from the NOE-derived structures and are reported as two entries each for G6 and C7.

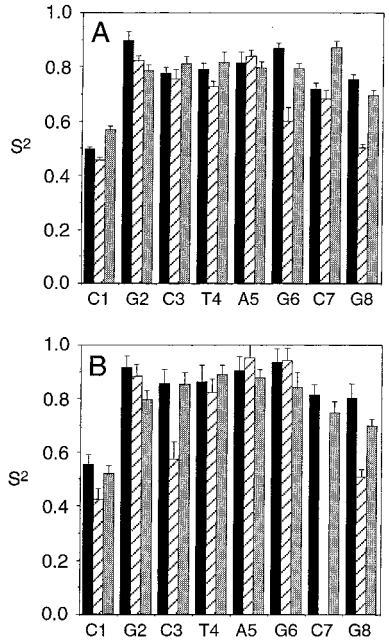

FIGURE 5: Dynamic parameters for CTSYM and CTSYMTOTO. For each residue in plots A and B, S^2-C1' is shown in solid black, S^2-C3' is striped, and S^2-C4' is gray: (A) order parameters for the deoxyribose methine carbons in CTSYM; and (B) order parameters for the deoxyribose methine carbons in CTSYMTOTO. Calculated error bars are shown.

extended *ap* conformation and the A5 ϵ torsion angle to adopt a $-sc$ conformation.

The order parameter for the CTSYMTOTO C3C3′ spin is significantly lower than those for the CTSYMTOTO C3C1′ and C3C4′ and the CTSYM C3C3′. The C3C3′ atom is connected to T4 through the five-bond C3′−O3′−P−O5′−C5′−C4′ backbone linkage that bridges the intercalation site. The difference observed for the order parameter for C3C3′ upon ligand association indicates a change in sequence-dependent structure-induced dynamic processes. Intercalation of TOTO changes the relative positioning of the G6-C7 bases, restricting the conformational freedom found for the CTSYM G6C3′, and simultaneously allowing the CTSYM-TOTO C3C3′ additional conformational freedom.

The CTSYMTOTO C3 deoxyribose is found to be in the O1′-endo conformation in the NOE-derived structures. The O1′-endo conformation is on the lowest-energy saddle point of the potential energy surface describing the deoxyribose pseudorotation cycle between the two low-energy C2′-endo and C3′-endo conformations (*37*). Conversion from the C2′-endo through the C1′-endo to the C3′-endo conformation is accompanied by significant displacements in the positions of the deoxyribose C2′ and C3′ carbons.

The highly disordered C3C3′ carbon in the presence of the highly ordered C3C1′, C4′, C6, and C5 carbons is indicative of a process where the C3′ carbon is moving with greater freedom than the base and the rest of the sugar. A potential source for the low order of the CTSYMTOTO C3C3′ is dynamic fluctuations in the torsions of the bonds between C3 and T4. There are three favored (allowed) torsions available to the each of the five backbone bond angles C3 ϵ, C3 ζ, T4 α, T4 β, and T4 γ that describe the conformation of the C3′−O3′−P−O5′−C5′−C4′ backbone linkage. However, not all combinations of the backbone angles are possible in the complex. Conformational changes about these bonds are coupled to the pseudorotation angles of the C3 and T4 deoxyribose residues. In normal B-form DNA, the *ap* conformation for the β and ζ torsion angles is higher in energy than either the $+sc$ or the $-sc$ conformations which allow back-bonding from the nonbonded phosphate oxygens into the phosphate ester bond (*37*).

A motional model for the C3 residue and internucleotide linkage can be proposed that combines a rapid equilibrium of the interresidue backbone conformation with the coupled exchange between the O1′-endo and the C2′-endo conformations. Molecular modeling using the NOE-derived restraints from the original structural study was employed to test this hypothesis. The NOE and H-bond restraints to the C3 residue were relaxed by $\pm$ 0.25 Å, and a torsional restraint was applied separately for each of the two additional possible rotamers of the backbone angles C3 ϵ and ζ, and T4 α, β, and γ spanning the intercalation site. Each of the 10 systems was subjected to the original RMD procedure, and the results were analyzed with the program CURVES 3.1. Each model was evaluated by superimposing the T4 C1′, C3′, C4′, and C6 and C3 C1′, C4′, and C6 atoms and measuring the displacement of the C3C3′ atom. Most changes in backbone torsional angles resulted in significant changes in atomic position for many of the atoms with high order parameters, indicating an incorrect model. However, when the T4 β was forced from (*ap*) to ($+sc$) only the C3C2′ and C3C3′ atoms

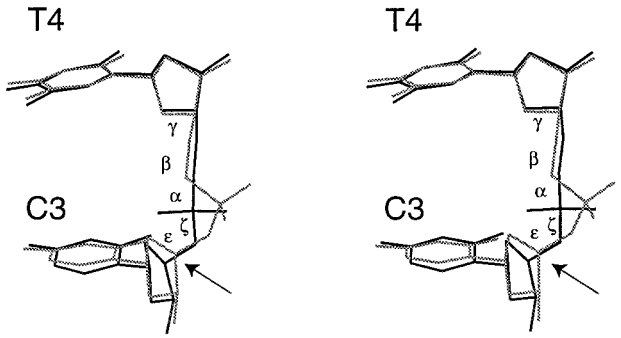

FIGURE 6: Superimposition of the CTSYMTOTO C3 and T4 residues from the original structural study (black) and the model after C3 β was forced from *ap* to +*sc* (gray). The displacement of C3C3′ is indicated by the arrow, and the backbone torsion angle designations are shown. The protons have been omitted for clarity.

were significantly displaced and the pseudorotation angle of C3 increased toward C2′-endo (Figure 6). Experimentally, the C4′−H4′, C1′−H1′, and C6−H6 bond vectors are found to have a much more restricted range of motions in this model with a maximum angular change of 20° for the C4′−H4′ bond vector (Table 4). The C3′ atom in this model is displaced up to 0.6 Å and the H3′ atom up to 1.0 Å. By using the simple motion in a cone model, all of the atoms except for the C3′ sweep out an angle of approximately 18° while the C3′ sweeps out a cone with a 34° arc. This is consistent with the atomic displacements in the O1′-endo and C2′-endo equilibration model. An alternative model that employs the equilibration of the deoxyribose between C2′-endo and C3′-endo is inconsistent with the pattern of the H1′−H2′ and H1′−H2″ cross-peaks in the DQF−COSY spectrum. Attempts were made to fit the observed cross-peak pattern to a rapidly equilibrating mixture of C2′-endo and C3′-endo conformations using spectral simulation (*38*). For the C3 deoxyribose in CTSYMTOTO, no self-consistent mixture of the two conformations could reproduce the observed cross-peak pattern (data not shown). The gross features of the H1′−H2′ and H1′−H2″ cross-peaks indicate that there is a significant C2′-endo conformational component.

^{31}P resonances of phosphates in the B_I ($\epsilon = 180°$, $\zeta = -90°$) conformation are found upfield from phosphate resonances in the B_{II} ($\epsilon = -90°$, $\zeta = 180°$) conformation (*39*). The CTSYMTOTO pG6 phosphate resonates at 2.76 ppm downfield from the pG2, pC7 (0.35 ppm), and pC3 and pG8 (0.54 ppm) resonances as well as downfield of the resonances for CTSYM (Figure 7). This downfield shift is indicative of both intercalation and a B_{II} phosphate conformation, while the other upfield-shifted resonances are at chemical shifts typical of "normal" B_I phosphates (*39*). The downfield pG6 phosphorus resonance is consistent with the observation of a relatively pure B_{II} conformation for the pG6 derived from analysis of the NOE-based structure (Table 5). The resonances for the pT4 and pA5 phosphates (1.10 ppm) are intermediate between the B_{II} pG6 and the upfield resonances of the "normal" phosphates. The pT4 bridges the pyrimidine side of the intercalation site, and the pA5 bridges the central TpA site. The calculated torsions from the NOE-derived structures indicate a relatively pure B_I conformation for both the pT4 and pA5. The appearance of the pT4 phosphate resonance at a chemical shift intermediate between B_I and B_{II} is consistent with a rapid conformational exchange

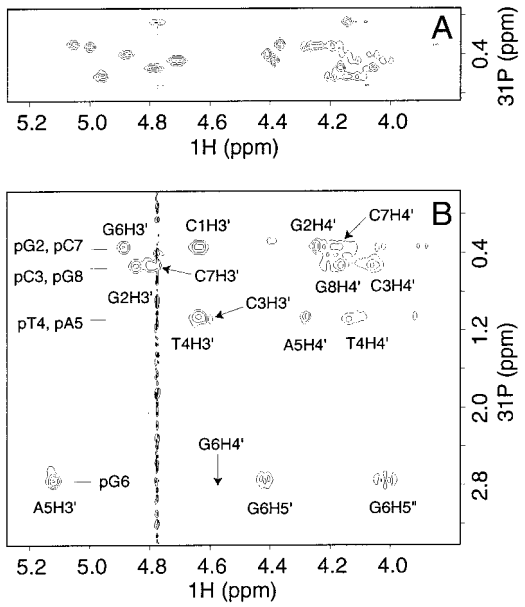

FIGURE 7: ^{1}H-^{31}P HSQC spectrum for CTSYM (A) and for CTSYMTOTO (B). The arrow indicates the chemical shift of the G6H4′. ^{31}P chemical shift values are relative to 85% phosphoric acid. The ^{1}H-^{31}P backbone correlations are shown as interresidue, 31P(*n*) H3′(*n* − 1); and intraresidue, 31P(*n*) H4′(*n*) and 31P(*n*) H5′/H5″(*n*). Cross-peaks due to the H5′/H5″ resonances are not labeled except for G6.

for the T4 β torsional angle leading to an averaged chemical shift. The intermediate chemical shift for the pA5 is also indicative of a process resulting from rapid exchange between B_I and B_{II} conformations. However, there are no indications from the order parameters or chemical exchange terms calculated for the T4 or A5 deoxyribose that suggest a potential motional model. On the basis of the backbone torsion angles calculated from the NOE-derived structure, the only phosphodiester linkage in the molecule that is clearly in the B_{II} conformation is pG6 which bridges the intercalation site on the purine step side. The remaining phosphodiester linkages in the CTSYMTOTO NOE-derived structure are in the B_I conformation, except for pG8 and pC7 which have an unusual set of conformations. The ^{31}P chemical shift for the pC7 and pG8 indicates that they are predominately in the B_I conformation. The torsions calculated for the pC7 from the NOE-derived structures fall into two equally populated sets of conformations and do not appear to be clearly in either the B_I or the B_{II} conformations. The most likely expanation for this observation is that there are insufficient NOE-derived restraints to define the backbone for the pC7 and pG8 linkages. It is also possible that the distortions introduced by the intercalation allow additional non-B_I or B_{II} conformations to be populated.

The backbone at the C3-p-T4 and A5-p-G6 steps must distort to accommodate the intercalation by TOTO. The T4 α torsion in the NOE-derived structures is found in the trans conformation typical of other intercalator-bound DNA. On the other hand, G6 $\alpha = -10°$ is in the *syn-periplanar* or cis conformation. To adopt this conformation, the G6H5′ and G6H5″ must point in toward and be in van der Waals contact with the chromophore. This unusual conformation calculated from the NOE structure is consistent with the spectral data. There are NOEs from the G6H5′ and G6H5″ protons to the chromophore protons and there is no cross-peak between the

pG6 and the G6H4′ in the ^{1}H-^{31}P HSQC spectrum (Figure 7b). The six other phosphates in the molecule have cross-peaks to their own H4′ in the ^{1}H-^{31}P HSQC spectrum. The unusual conformation at the G6 γ torsion prevents good orbital overlap of the bonds that would allow an observable coupling between the phosphorus and the H4′.

Commentary on the Drug. The order parameters for the spins on the aromatic portion of the drug are uniformly high and in the range of the CTSYM aromatic order parameters. None of the drug spins required a chemical exchange term to fit the relaxation data indicating a quite rigid structure (vide infra). The observed quenching of the DNA dynamics by binding of TOTO can be rationalized by the aromatic dye acting as a splint across the Watson−Crick base-pairing edge junction of the base pair. Potential motions that could be inhibited by this splint include dynamic changes in buckle and propeller twist. The fluorescence quantum yield of TOTO is enhanced by more than 3000-fold upon binding to dsDNA. Clamping of the TOTO chromophore between the dsDNA base pairs prevents the free rotation of the benzothiazole ring about the methine bonds relative to the quinolinium ring. This rotation is possible in uncomplexed TOTO allowing relaxation of the photochemically excited state nonradiatively. When bound to dsDNA the two halves of the chromophore are held much more rigidly, and the chromophore loses excitation energy by fluorescence instead. The relatively high order of the spins in the chromophore indicates that there is very little freedom to rotate and lose photochemical excitation energy nonradiatively.

Chemical Exchange in the CTSYM and CTSYMTOTO. There are a number of spins that require the inclusion of a significant R_{ex} term for an adequate fit to the experimental data to a dynamic model (Tables 3 and 4). The inclusion of an R_{ex} term in the model-free formalism generally accounts for such effects as chemical exchange and conformational averaging. However, the R_{ex} values reported here are not directly measured and are the results of correction terms to R_2 experimental data to achieve a better fit between theory and experiment. Even so, a relatively large R_{ex} value may indicate the existence of an intramolecular conformational exchange process. In numerous studies on the backbone dynamics in proteins, values of $R_{ex} > 1$ Hz are considered significant and imply that these spins undergo significant dynamic processes in the microsecond to millisecond time regime. Using these criteria, we find that 12 of the 36 spins in the CTSYM have significant microsecond to millisecond dynamic processes (Figure 4c). Of the 45 spins that were analyzed for the CTSYMTOTO, only three spins showed significant microsecond to millisecond dynamic processes, two deoxyribose spins and the terminal G8C8 (Figure 4d).

The formation of the drug−DNA complex quenches most of the chemical exchange components required to fit the relaxation data to the model-free formalism for the entire molecule, suggesting a freezing out of microsecond to millisecond time scale conformational heterogeneity upon complex formation (Figure 4b,d). Structurally, this can be rationalized by the significant stacking interactions observed between the bases and the TOTO in the CTSYMTOTO structure and the increased DNA−base−DNA−base stacking interactions brought on by the underwinding of the helix in the complex (Figure 4b,d). The overlap of neighboring bases is increased going from the canonical B-form conformation of CTSYM to the distorted conformation of CTSYMTOTO. Analysis of the CTSYMTOTO structure (*20*) shows that there are large chromophore−base interaction surfaces for all four nucleotides in the intercalation site.

Previous ^{1}H NMR studies have shown that adenine bases at TpA steps experience large amplitude (20°−50°) microsecond to millisecond time scale motions (*40*−*42*). These dynamics are thought to arise from poor stacking interactions at this step. The order parameters for the aromatic and sugar spins in the central TpA base-pair step for the CTSYM are very high. However, there are significant chemical exchange components calculated for these spins. TpA base-pair steps are the thermodynamically least stable of the base-pair steps (*43*−*44*) due in part to poor stacking interactions. This instability does not seem to manifest itself as disorder on the picosecond to nanosecond time scale, rather as significant microsecond to millisecond time scale dynamics. We have observed similar evidence for microsecond to millisecond dynamics at the central TpA step in our previous study of $d(GCGTACGC)_2$ (*10*). Only the TpA aromatic spins showed microsecond to millisecond dynamics in that alternating purine−pyrimidine sequence.

The chemical exchange for the TpA in CTSYM is quenched upon TOTO complex formation. The unwinding of the helix to accommodate the bis-intercalation increases the surface area of adjacent base pairs that are in mutual contact. The central TpA sandwiched by the drug is unwound to 25° in CTSYMTOTO. The underwinding in the TOTO complex at the TpA step substantially increases the total area involved in π stacking of the adjacent thymine and adenine bases. Additional evidence for the clamping of the TpA site in CTSYMTOTO and reduction in dynamic processes was observed in the previous structural study through the observation of the adenine 6-amino protons in H_2O spectra. These resonances are almost always absent in normal DNA spectra due to exchange processes.

The only aromatic spin in CTSYMTOTO to require a chemical exchange term is the terminal G8C8. The G8 deoxyribose order parameters are reasonably high, and there are no R_{ex} terms required for the G8 deoxyribose spins. The C1-G8 base pair is three nucleotides away from the intercalator in the complex. The R_{ex} term of the G8C8 spin may reflect destabilization of the DNA as it makes the transition from a distorted TOTO complex conformation back to a normal B-form conformation or an end-of-helix fraying effect.

Formation of a covalent psoralen monoadduct to one of thymidines in $d(GCGTACGC)_2$ quenches most of the observed microsecond to millisecond dynamics where substantial stacking interactions between the drug and DNA bases are present (*10*). Poor stacking between the intercalated psoralen adduct and one of the adjacent bases leads to significant dynamics for that base on the microsecond to millisecond time scale (*10*). In contrast to the undamaged $d(GCGTACGC)_2$, most of the bases in CTSYM show dynamics on the microsecond to millisecond time scale. In both of these unmodified DNA molecules the thermodynamic destabilization of the TpA step does not manifest itself in the calculated order parameters, rather in the chemical exchange terms. These results highlight the effect of sequence on the observed dynamics in DNA systems.

There are only three atoms in the CTSYMTOTO that require the inclusion of a chemical exchange term in order to fit the relaxation data, and the A5C3′ is the only atom in a nonterminal residue. There is a significant increase in the chemical exchange term for the A5C3′ upon TOTO complex formation, changing from 3 ± 1 to 7 ± 2 s^{-1}. The A5C3′ atom is attached to the pG6 phosphate that bridges the binding site between A5 and G6. Interestingly, the order parameters for this atom and all of the other deoxyribose atoms in A5 and G6 are very high. However, the chemical exchange term indicates that there are motions available to A5C3′ in response to the TOTO binding that may be analogous to those described above for the C3C3′ only on a longer time scale. The differences in the time scales may be due to the steric interactions of the linker chain with the A5-G6 step. Congestion due to the bulk of the linker pressing on the A5 deoxyribose in the purine−purine side of the binding site may interfere with the more free motions available to the backbone on the more open pyrimidine−pyrimidine side of the binding site.

Motional Model for the Nucleotide Residues. The purine C8 and pyrimidine C6 atom order parameters for the CTSYM and CTSYMTOTO show a reasonable correlation between S^2 for the C1′ and aromatic spins. The S^2 values for the C5 and C6 spins in each of the cytosine bases in the CTSYM and CTSYMTOTO are different. The largest difference is for the CTSYM C7C6 and C7C5 atoms. This is interesting because the values bracket the relatively low S^2 for the CTSYM C7C1′. In both the CTSYM and the CTSYMTOTO the C7C5 atom is less ordered than the adjacent C7C6 atom. While these cytosine base atoms are covalently connected as part of a rigid aromatic system, the CH bond vectors point in different directions. Pivoting of the base around the glycosidic bond should subject the C6−H6 and the C5−H5 bond vector to the same amplitude motions on an identical time scale. In a simple motional model, the direct attachment of the C1′ to the base means that translational motions of the base equally affect the order of the adjacent C1′ spin. In this model, only rotations about the glycosidic bond, χ, could make S^2(C1′) different from S^2(C8, 2, 6, 5). These results suggest that a more complicated motional model must be considered to account for the observed discrepancy. An additional possibility may be that the value for the CSA tensor for the C5 and C6 may be significantly different, leading to different relaxation behavior. Model-free calculations performed with the CSA for the pyrimidine C5 set to 140 ppm instead of 185 ppm resulted in order parameters for the C5 spin almost identical to that for the C6 spin. Unfortunately, neither are the true values of the CSA tensors known nor are the current data sufficient to develop a more complex model that is valid in these systems. Similar differences for the cytosine C5 and C6 order parameters were observed in the d(GCGTACGC)$_2$ (*10*).

DISCUSSION

The solution structure of the CTSYMTOTO has been determined by NOE-driven methods and gives a high-resolution time-averaged picture of the organization of the CTAG sequence where the TOTO binding has its greatest impact (*20*). Examination of the order parameters for the CTSYM and CTSYMTOTO reveals a complex pattern of dynamics. Dynamic parameters were determined for the methine carbons in most of the residues in these systems. Deoxyribose is known to interconvert between different conformations related by pseudorotation of the furanose ring resulting in the displacement of ring atoms on the picosecond to microsecond time scale, exactly where ^{13}C relaxation analysis is sensitive. The deoxyribose C3′ atom undergoes a large displacement during the conformational exchange between C2′-endo (B-form) and C3′-endo (A-form). Because the different sugars and the atoms within the sugars have radically different S^2 values, in favorable cases we can use this information and COSY type data to select models that describe the equilibration between different pseudorotation conformers.

Molecules that bind to DNA by intercalation form an important class of chemotherapeutic and diagnostic compounds. The binding of intercalators to DNA lengthens the helix and results in an overall stiffening of the DNA duplex as monitored by enhanced viscosity and diminution of the sedimentation coefficient. The usefulness of thiazole orange as a building block for designed DNA ligands is dependent on understanding the factors that are responsible for binding and the dynamic exchange of the dye between sites. The tight binding and limited flexibility of the CTSYMTOTO complex as evidenced by the high order parameters and quenching of chemical exchange terms are probably important for the brightness of TOTO as a fluorescent probe for dsDNA.

The observation that binding of TOTO to the DNA alters the microsecond to millisecond dynamics in the bases that are not in the actual CTAG intercalation site provides insight into the mechanism of intercalative chemotherapeutic drugs. Intercalation provides a large surface area between the chromophore and the DNA which can provide a substantial free energy of binding. The DNA metabolism altering effects of these drugs may not just be limited to the local disruption of DNA structure at the site of binding by altering the geometry of the DNA and/or the introduction of inappropriate steric bulk by the drug. The current study shows that changes in helix dynamics and structure may be propagated away from the DNA−drug binding site through the progressive conformational changes required for the DNA to return to an undistorted B-form conformation. Subtle changes in dynamic behavior may be transmitted a significant distance down the polymer away from the site of drug−DNA interaction because DNA is plastic and can be readily deformed by the binding of ligands. This effect may manifest itself as alterations in the binding constant of ligands remote from the site of drug−DNA interaction. Thus, the binding of a drug to one site on a DNA molecule can affect the affinity of a different ligand for an adjacent DNA sequence. There are numerous amino acid contacts to the backbone phosphates observed in high-resolution X-ray crystal structures of protein−DNA complexes (*45*). The flexibility of the phosphate esters in the recognition and formation of protein−DNA contacts has been proposed as a mechanism for discrimination of different operator sites by the lac repressor (*46*−*47*). Flexibility of the backbone is a more general case of localized sequence-specific conformational variations in DNA that are potentially recognized by proteins. Consequently, the effects of drug−DNA complexes may be less local than is apparent by inspection of the structure of a complex.

Dynamic processes or "fraying" is often invoked to account for anomalies in NOE intensities for terminal nucleotides in DNA oligomers. We find that the 5′−C1 deoxyribose carbons are very disordered. This is in contrast to the d(GCGTACGC)$_2$ where the 5′−G1 deoxyribose is reasonably ordered. The order parameters for the CTSYM and CTSYMTOTO aromatic spins are uniformly high except for the 3′-terminal G in both molecules. In our previous study we found that the 3′-terminal C8 deoxyribose spins for d(GCGTACGC)$_2$ are on average lower than for the rest of the molecule (*10*). Borer et al. (*11*) found that the base order parameters for the terminal nucleotides are lower than for the central residues in the hexamer d(CGCGCG)$_2$, which under the conditions studied had a melting temperature similar to those of the CTSYM and d(GCGTACGC)$_2$. The order parameters measured in this study and in the previous study (*10*) are generally much higher than those found by Borer et al. (*11*). This suggests that "end effects" involving high-frequency internal motions are sequence-dependent. On the other hand, the spins in the deoxyribose residues show a much greater sequence-dependent variation in order parameters. In Borer et al., the data was collected by direct detection of ^{13}C by 1D NMR for NOE and R_1. The present study involved the measurement of a third parameter R_2, which allows for a more complete description of the system. The studies on these molecules point out the likelihood that there are significant sequence-dependent variations in internal DNA dynamics. The values found for the effective internal correlation time, τ_f, in the CTSYM and CTSYMTOTO, which range up to 80 ps, agree with the values estimated by Borer et al. (*11*) for sugar and base motions (30−300 ps) and with those of Gaudin et al. (*12*) for an internal diffusion coefficient of 30×10^7 s^{-1} for a restricted rotation model about the glycosidic bond with $\Delta\chi = 28°$. It is possible that the DNA forms transient end-to-end stacked aggregates at the relatively high DNA concentrations used in these studies, which may alter the motional freedom of the terminal residues. However, the self-consistent theoretical, homo- and hetero-nuclear-derived τ_m values argue against this being a major effect. Differences in results may also reflect sequence-dependent effects.

The pulse sequence used to measure R_2 in this study does not account for the cross correlation (interference) between the CSA and dipolar relaxation mechanisms. The cross correlation for aliphatic carbons can be neglected because the CSA contribution to relaxation is small compared to the dipolar contribution. Because the CSA for the aromatic carbons is much larger, there is a correspondingly larger interference between the CSA and dipolar relaxation mechanisms. The magnitude of this interference on R_2 can be calculated (*27*). For the aromatic carbons, the calculated effect would increase the measured R_2 by approximately 24% for a CSA of 185 ppm and 4% for a CSA of 41 ppm. The conclusions of the study are not altered if these adjusted numbers are used in the calculations of S^2. However, the calculated order parameters for the aromatic spins are slightly higher.

The current analysis is a limited description of the dynamic modes that characterize the complex conformational equilibria of these two DNA molecules in solution. The primary limitation of this approach is that the complex equilibria are oversimplified by the model-free approach, and because the problem is in general underdetermined. However, the results obtained in this study suggest that model-free analysis coupled with the physical constraints of the system being studied can yield tentative physical models for motion. For each sugar residue under ideal conditions, order parameters for the three ring methine carbons can be determined and the base C8, C6, C2, and C5 carbon order parameters can be correlated with the sugar residue through the motion of the base relative to the sugar about the glycosidic bond. The constraints imposed on the system by these coupled order parameters allow us to constrain the potential motions available to the polymer by more than simply attempting to rationalize the significance of the order parameters for the individual C−H vectors alone in isolation. This is demonstrated for the proposed model for conformational exchange for the CTSYMTOTO C3 deoxyribose between C2′-endo and C1′-exo conformations. More complete motional models can be tested by mapping the spectral density function of the spins. However, this approach requires further investigation with ^{13}C isotopically enriched molecules.

Biological Consequences. We are in a position to begin a structure−dynamics correlation analysis to determine the role conformational heterogeneity of the DNA target has in the binding of ligands. The description of the dynamic processes available to the TOTO−DNA complex combined with the high-resolution solution structure already available may allow us to manipulate the sequence selectivity of the ligand. Analogues can be designed and synthesized that take advantage of the conformational characteristics revealed by the structure to modulate the effects on the dynamics of the DNA. It will be possible to test the effect of additional functional groups on the dynamic processes and whether specific backbone conformations can be induced on the more conformationaly mobile pyrimidine side of the binding site. This is important because many therapeutic compounds are thought to act by interacting with DNA as their ultimate target. Protein−DNA interactions may be mediated by dynamic processes in the DNA backbone such as those described for the CTSYMTOTO-C3 and CTSYM-G6 residues. This is a further example of the power in dynamic analysis of DNA molecules. These data may be useful in the design of new ligands and an understanding the sequence selectivity of DNA−ligand interactions.

ACKNOWLEDGMENT

We thank Professor Jöel Mispelter (INSERM, Orsay) for providing the pulse sequences that we modified to accomplish this work, Professor Arthur G. Palmer, 3rd (Columbia University, New York), for providing ModelFree and many helpful discussions, and Dr. Jens Peter Jacobsen (Odense University, Odense, DK) for the providing the CTSYMTOTO sample and for careful reading of the manuscript.

REFERENCES

1. Jacobsen, J. P., Pedersen, J. B., Hansen, L. F., and Wemmer, D. E. (1995) *Nucleic Acids Res. 23*, 753−760.
2. Hansen, L. F., Jensen, L. K., and Jacobsen, J. P. (1996) *Nucleic Acids Res. 24*, 859−867.

3. Brooks, C. L., III, Karplus, M., and Pettitt, B. M. (1988) *Proteins: A Theoretical Perspective of Dynamics, Structure and Thermodynamics*, J. Wiley and Sons, New York.
4. Bax, A., Sparks, S. W., and Torchia, D. A. (1989) *Methods Enzymol. 176*, 134−150.
5. Nirmala, N. R., and Wagner, G. (1988) *J. Am. Chem. Soc. 110*, 7557−7558.
6. Palmer, A. G., 3rd, Rance, M., and Wright, P. E. (1991) *J. Am. Chem. Soc. 113*, 4371−4380.
7. Palmer, A. G., 3rd, Hochstrasser, R. A., Millar, D. P., Rance, M., and Wright, P. E. (1993) *J. Am. Chem. Soc. 115*, 6333−6345.
8. Alattia, T., Padilla, A., and Cavè, A. (1996) *Eur. J. Biochem. 237*, 561−574.
9. Mispelter, J., Lefevre, C., Adjadj, E., Quiniou, E., and Favaudon, V. (1995) *J. Biomol. NMR 5*, 233−244.
10. Spielmann, H. P. (1998) *Biochemistry 37*, 5426−5438.
11. Borer, P. N., LaPlante, S. R., Kumar, A., Zanatta, N., Martin, A., Hakkinen, A., and Levy, G. C. (1994) *Biochemistry 33*, 2441−2450.
12. Gaudin, F., Paquet, F., Chanteloup, L., Beau, J. M., Nguyen, T. T., and Lancelot, G. (1995) *J. Biomol. NMR 5*, 9−58.
13. Hogan, M. E., and Jardetzky, O. (1979) *Proc. Natl. Acad. Sci. U.S.A. 76*, 6341−6345.
14. Hogan, M. E., and Jardetzky, O. (1980) *Biochemistry 19*, 2079−2085.
15. Hogan, M. E., and Jardetzky, O. (1980) *Biochemistry 19*, 3460−3468.
16. Keepers, J. W., and James, T. L. (1982) *J. Am. Chem. Soc. 104*, 929−939.
17. Kochoyan, M., Leroy, J. L., and Gueron, M. (1987) *J. Mol. Biol. 196*, 599−609.
18. Gueron, M., Kochoyan, M., and Leroy, J. L. (1987) *Nature 328*, 89−92.
19. Briki, F., Ramstein, J., Lavery, R., and Genest, D. (1991) *J. Am. Chem. Soc. 113*, 2490−2493.
20. Spielmann, H. P., Wemmer, D. E., and Jacobsen, J. P. (1995) *Biochemistry 34*, 8542−8553.
21. Lavery, R., and Sklenar, H. (1988) *J. Biomol. Struct. Dyn. 6*, 63−91.
22. Lavery, R., and Sklenar, H. (1989) *J. Biomol. Struct. Dyn. 6*, 655−667.
23. Staerk, D., Hamed, A. A., Pedersen, E. B., and Jacobsen, J. P. (1997) *Bioconjugate Chem. 8*, 869−877.
24. Delsuc, M. A., and Lallemand, J. Y. (1986) *J. Magn. Reson. 69*, 504−507.
25. States, D. J., Haberkorn, R. A., and Ruben, D. J. (1982) *J. Magn. Reson. 48*, 286−292.
26. Schmieder, P., Ippel, J. H., van den Elst, H., van der Marel, G. A., Altona, C., and Kessler, H. (1992) *Nucleic Acids Res. 20*, 4747−4751.
27. Palmer, A. G., 3rd, Skelton, N. J., Chazin, W. J., Wright, P. E., and Rance, M. (1992) *Mol. Phys. 75*, 699−711.
28. Abragam, A. (1968) *The principles of Nuclear Magnetism*, Clarendon Press, Oxford, U.K.
29. Williamson, J. R., and Boxer, S. G. (1988) *Nucleic Acids Res. 16*, 1529−1540.
30. Lipari, G., and Szabo, A. J. (1982) *J. Am. Chem. Soc. 104*, 4546−4559.
31. Lipari, G., and Szabo, A. J. (1982) *J. Am. Chem. Soc. 104*, 4559−4570.
32. Clore, G. M., Szabo, A., Bax, A., Kay, L. E., Driscoll, P. C., and Gronenborn, A. M. (1990) *J. Am. Chem. Soc. 112*, 4989−4991.
33. Bloom, M., Reeves, L. W., and Wells, E. J. (1965) *J. Chem. Phys. 42*, 1615−1624.
34. Mandel, A. M., Akke, M., and Palmer, A. G., 3rd. (1995) *J. Mol. Biol. 246*, 144−163.
35. Liu, H., Spielmann, H. P., Ulyanov, N. B., Wemmer, D. E., and James, T. L. (1995) *J. Biomol. NMR 6*, 390−402.
36. Eimer, W., Williamson, J. R., Boxer, S. G., and Pecora, R. (1990) *Biochemistry 29*, 799−811.
37. Saenger, W. (1984) *Principles of Nucleic Acid Structure*, Springer-Verlag, New York.
38. Macaya, R. F., Schultze, P., and Feigon, J. (1992) *J. Am. Chem. Soc. 114*, 781−783.
39. Gorenstein, D. G. (1994) *Chem. Rev. 94*, 1315−1338.
40. Kennedy, M. A., Nuutero, S. T., Davis, J. T., Drobny, G. P., and Reid, B. R. (1993) *Biochemistry 32*, 8022−8035.
41. Lingbeck, J., Kubinec, M. G., Miller, J., Reid, B. R., Drobny, G. P., and Kennedy, M. A. (1996) *Biochemistry 35*, 719−734.
42. McAteer, K., Ellis, P. D., and Kennedy, M. A. (1995) *Nucleic Acids Res. 23*, 3962−3966.
43. Allawi, H. T., and SantaLucia, J. (1997) *Biochemistry 36*, 10581−10594.
44. SantaLucia, J., Jr., Allawi, H. T., and Seneviratne, P. A. (1996) *Biochemistry 35*, 3555−3562.
45. Beamer, L. J., and Pabo, C. O. (1992) *J. Mol. Biol. 227*, 177−196.
46. Botuyan, M. V., Keire, D. A., Kroen, C., and Gorenstein, D. G. (1993) *Biochemistry 32*, 6863−6874.
47. Karslake, C., Botuyan, M. V., and Gorenstein, D. G. (1992) *Biochemistry 31*, 1849−1858.

BI980789E